^{1}H NMR Studies of Sarafotoxin SRTb, a Nonselective Endothelin Receptor Agonist, and IRL 1620, an ET_B Receptor-Specific Agonist[†,‡]

Annette R. Atkins, Rodney C. Martin,[§] and Ross Smith*

Biochemistry Department, University of Queensland, Queensland 4072, Australia

Received September 12, 1994; Revised Manuscript Received November 10, 1994[⊗]

ABSTRACT: ^{1}H NMR studies on the nonselective endothelin receptor agonist sarafotoxin SRTb have identified a helix between residues Asp 8 and His 16, and a β-turn involving residues Cys 3 to Met 6; however, the biologically important C-terminal five residues were found to be conformationally variable. The average RMSD, measured for the final 43 refined structures to the average structure over residues 1−16, was 0.78 ± 0.18 Å for the backbone atoms and 1.39 ± 0.22 Å for all atoms. The torsion angles Cys 3 ψ/Lys 4 ϕ, Thr 7 ψ/Asp 8 ϕ, and Gln 17 ϕ were identified as sites of conformational variability. Differences were found between the structures in the bicyclic loop region for SRTb and those published for ET1, another nonselective receptor agonist, which may explain the observed differences in potency of these peptides. The conformation of an ET_B receptor-specific agonist, IRL 1620, which lacks the N-terminal seven residues and the two intrachain disulfides, was found by NMR and circular dichroism spectroscopy to be predominantly random coil, despite the fact that its affinity for the ET_B receptor almost equals that of ET1. However, close analysis of the NMR results indicated the presence of turn-like structures, or a nascent helix, in the part of the sequence corresponding to the helical region in the parent peptides. These results suggest that the helical conformation may be required for ligand binding to the ET_B receptor as well as to the ET_A receptor.

The mammalian endothelins (ETs)[1] (Yanagisawa et al., 1988) and the snake venom sarafotoxins (SRTs) (Kloog et al., 1988) comprise a family of potent vasoactive peptides, characterized by a highly conserved, 21 amino acid sequence with two intrachain disulfide bonds. The nonconservative amino acid substitutions that do occur across the family are predominantly in the region between residues 4 and 7, contrasting with the high homology of the C-terminal hexapeptides.

Extensive studies have been undertaken to determine the three-dimensional conformation of these peptides using high-resolution NMR (e.g., Mills et al., 1994, 1992; Andersen et al., 1992a; Aumelas et al., 1991; Bortmann et al., 1991; Tamaoki et al., 1991), circular dichroism (CD) (Atkins et al., 1994; Tamaoki et al., 1992; Bennes et al., 1990; Saudek et al., 1990), and fluorescence (Pelton, 1991) spectroscopies. The NMR studies have not revealed a peptide fold common to the whole family, but consistent structural features have been identified, including an extended conformation for the first three or four residues, a turn-like structure [centered at residues 5−8 in endothelin-1 (ET1)], and a helix, or helix-like structure, between residues 9 and 15 or 16. However, the biologically important and highly conserved C-terminal hexapeptides were found to be conformationally flexible in the majority of the studies. A recently published crystal structure of ET1 (Janes et al., 1994) found the N-terminal residues in a similar extended β-strand conformation; however, the C-terminal segment was found to be an irregular helix, in conflict with both the NMR and CD results.

These peptides elicit their cellular responses on binding to specific membrane-bound receptors (Sokolovsky et al., 1992), three subtypes of which have been identified based on ligand binding specificity. The ET_A receptor binds ET1 with higher affinity than endothelin-3 (ET3) or the SRTs, the ET_B receptor binds each of the isopeptides with similar affinity, while the ET_C receptor selectively binds ET3 (Karne et al., 1993). Mutation and truncation studies have shown that the entire three-dimensional structure of the peptides is required for binding to the ET_A receptor, whereas only residues 10−21 are necessary for effective binding to the ET_B receptor (Saeki et al., 1991). The structural requirements of the ET_C receptor have not been identified.

Since the initial classification of the endothelin receptor subtypes, receptor-specific agonists and antagonists have been identified, allowing more detailed analysis of the receptor−ligand interactions. We report here structural studies on a nonselective ligand, SRTb, which has 67% homology with ET1 and binds with moderate affinity to the ET_A receptor [IC_{50} SRTb 0.95 nM, ET1 0.16 nM; porcine aortic smooth muscle membranes (Saeki et al., 1991)], and on IRL 1620, an ET_B-specific agonist (Takai et al., 1992).

[†] This work was supported by a Postgraduate Biomedical Research Scholarship from the National Health and Medical Research Council and a British Council Bursary to A.R.A.

[‡] Coordinates for the 10 lowest-energy structures have been deposited in the Protein Data Bank and assigned the identity code 1SRB.

* Address for correspondence: Ross Smith, Biochemistry Department, University of Queensland, Queensland 4072, Australia. Telephone: 61 7 365 4627. Fax 61 7 365 4699. E-mail ross@biosci.uq.oz.au.

[§] Current address: Centre for Drug Design and Development, Gehrmann Laboratories, University of Queensland, Queensland 4072, Australia.

[⊗] Abstract published in *Advance ACS Abstracts,* January 15, 1995.

[1] Abbreviations: CD, circular dichroism; DQF-COSY, double-quantum filtered correlated spectroscopy; ET, endothelin; HBTU, 2-(1-*H*-benzotriazol-1-yl)-1,1,3,3-tetramethyluronium hexafluorophosphate; NOE, nuclear Overhauser effect; NOESY, nuclear Overhauser effect spectroscopy; PAM, 4-(oxymethyl)phenylacetamidomethyl; RMSD, root mean squared deviation; SRT, sarafotoxin; TOCSY, total correlated spectroscopy; TPPI, time-proportional phase incrementation.

0006-2960/95/0434-2026$09.00/0

IRL 1620 is an N-terminally truncated derivative, which binds with similar affinity to ET_B receptors as ET1 (K_i ET1 8 pM; K_i IRL 1620 16 pM), but binds only weakly to ET_A receptors (K_i ET1 40 pM; K_i IRL 1620 1900 nM).

MATERIALS AND METHODS

SRTb was synthesized and purified as described previously (Atkins et al., 1994). IRL 1620 was prepared by manual solid-phase synthesis using tBoc-protected amino acids and a polystyrene resin with the C-terminal tryptophan attached through a 4-(oxymethyl)phenylacetamidomethyl (PAM) linker. The amino acids were activated as 2-(1-*H*-benzotriazol-1-yl)-1,1,3,3-tetramethyluronium hexafluorophosphate (HBTU) esters and coupled with *in situ* neutralization (Schnölzer et al., 1992). The extent of amino acid coupling was monitored using the ninhydrin reaction (Sarin et al., 1981). N-terminal succinylation was accomplished while the peptide was attached to the resin using succinic anhydride in the presence of triethylamine at 298 K. The peptide was cleaved from the resin, and the side chains were deprotected using anhydrous hydrogen fluoride at 268 K in the presence of *p*-cresol and *p*-thiocresol as radical scavengers. The peptide was purified initially on a low pressure C_{18} column using an increasing acetonitrile/0.1% trifluoroacetic acid (TFA) gradient in water and, subsequently, using the same solvent system, by HPLC on a 8 mm × 100 mm C_{18} column. The identity of the purified peptide was established by electrospray mass spectroscopy (experimentally determined 1821.5 mu compared to theoretical 1822 amu), and its biological activity was confirmed on rat airway tissues (S. R. O'Donnell and C. S. Kay, unpublished results).

Peptide solutions were prepared in water and quantified using molar extinction coefficients SRTb $\epsilon_{279} = 7250\ M^{-1}\ cm^{-1}$ (Pelton, 1991), IRL 1620 $\epsilon_{280} = 7000\ M^{-1}\ cm^{-1}$ (Gill et al., 1989).

NMR experiments were performed on a Bruker AMX 500 spectrometer. Low temperature operation of the spectrometer was achieved by passing a stream of cold N_2 over the sample and regulating the temperature with the probe heater. Chemical shifts were referenced to 3-trimethylsilylpropionic acid-d_4 (Fluka). Phase-sensitive DQF COSY (Rance et al., 1983), TOCSY (Braunschweiler et al., 1983), and NOESY (Jeener et al., 1979) spectra were recorded using TPPI for quadrature detection in F_1 (Marion et al., 1983). Water suppression was achieved with low power saturation during the recycle delay of 1.8 s and during the mixing time of the NOESY experiment. Spectra were typically recorded with 6 kHz spectral width and were collected as 512 t_1 increments into 4096 memory locations. Processing was done with UXNMR and involved a single zero fill and a shifted sine-bell apodization in both F_1 and F_2, followed by baseline correction using a third-order polynomial. Assignment of the spectra and volume integration of the NOESY cross peaks was accomplished using the EASY package (Eccles et al., 1989). Coupling constants were measured for amide protons from 1D experiments recorded with high digital resolution (0.4 Hz/point), and for $\alpha\beta$ protons from slices through 8192 × 512 DQF COSY spectra.

Spectra of SRTb were recorded at 2.2 mM, ~pH 3, and 303 K in either 10% D_2O/90% H_2O or 100% D_2O. Mixing times of 250, 300, and 350 ms were used in the NOESY experiments. The MLEV-17 pulse sequence, with a spin lock field of 8 kHz and a mixing time of ~80 ms, was used for the TOCSY. IRL 1620 was prepared as a 2.4 mM solution in the same solvents as used for SRTb, and spectra were recorded at 280 and 284 K and pH 6.6−7.1. NOESY spectra were acquired at mixing times of 300 and 350 ms.

NOE cross peak volumes for SRTb were converted to the distance restraints of 2.8, 3.5, and 5.0 Å by comparison of the volumes for the helical region between residues 9 and 15 with the theoretical distances expected in α-helices. Appropriate pseudoatom corrections were applied where stereospecific assignments were not available (Wüthrich et al., 1983).

Structure calculations for SRTb were performed using X-PLOR version 3.1 (Molecular Simulations, Inc., Burlington, MA) on a Sun SPARCstation2. *Ab initio* simulated annealing was used to generate structures which satisfied the experimental restraints. The starting structures, generated from a template by randomizing the ϕ and ψ angles, were initially energy minimized in a geometric force field (k_{bond} = 500 kcal mol^{-1} $Å^{-2}$, k_{ang} and $k_{improper}$ = 500 kcal mol^{-1} rad^{-2}) with a purely repulsive, nonbonded energy term (repel = 1, weight = 0.002), a soft square-well NOE restraining function (k_{NOE} = 50 kcal mol^{-1} $Å^{-2}$, asymptote = 0.1), and an energy constant of 5 kcal mol^{-1} rad^{-2} for the experimental dihedral angle restraints. The structures were then subjected to a total of 30 ps of dynamics calculations at 1000 K in two stages. Reduced weightings on the van der Waals (0.002), angle (0.4), and improper terms (0.1) were employed during the initial 20 ps to facilitate extensive sampling of conformational space. In the second stage of 10 ps, the weighting on the the angle and improper terms and the asymptote of the soft square well NOE function were increased to 1.0. Structures were then cooled to 100 K over 15 ps as the van der Waals radii and weighting were gradually reduced and increased, respectively (final repel = 0.8, final weighting = 4.0). An increased energy constant for the experimental dihedral restraints (k_{cdih} = 200 kcal mol^{-1} rad^{-2}) was also employed for this annealing step. During these initial structure calculations, the disulfide bonds were explicitly deleted and included only as distance restraints.

Structures were refined with a second round of simulating annealing from 1000 to 100 K over 10 ps, during which the disulfide bonds were explicitly defined. The energy constants from the geometic force field specified above were used, in conjunction with a square-well NOE restraining function (k_{NOE} = 50 kcal mol^{-1} $Å^{-2}$), and an energy constant of 200 kcal mol^{-1} rad^{-2} for the experimental dihedral angle restraints. The van der Waals radii and weighting term were varied during the calculations as explained for the first round of simulated annealing.

The refined structures were subsequently energy minimized for 500 steps in a force field based on the CHARMm force field. A Lennard-Jones potential was used to describe the van der Waals function, with a switching function employed to force the nonbonded energy smoothly to zero at 7.5 Å. The hydrogen bond and dihedral energy terms were calculated, as defined in the X-PLOR manual using the default parameters, and reduced energy constants were used for the experimental restraints (k_{NOE} = 10 kcal mol^{-1} $Å^{-2}$ and k_{cdih} = 50 kcal mol^{-1} rad^{-2}).

Circular dichroism spectra of IRL 1620 were recorded on a Jasco 720 spectropolarimeter between 250 and 185 nm, with a 1.0 nm bandwidth, 1 s response time, averaged over 5 scans, at a scan rate of 20 nm min^{-1} or 50 nm min^{-1}. The

Table 1: Chemical Shifts[a] and Coupling Constants[b] of SRTb at 303 K and pH 3.0

		chemical shift			coupling constants	
residue	NH	αH	ββ′	others	$^3J_{N\alpha}$	$^3J_{\alpha\beta}$
Cys 1		4.22	3.32, 3.13			4.0, 9.5
Ser 2	8.93	4.74	3.84		8.6	
Cys 3	8.74	4.95	3.36, 2.92		8.5	5.0, 10.5
Lys 4	8.11	4.13	1.71	γ1.36, δ1.41, ϵ 2.97, NH 7.50		
Asp 5	8.75	4.55	3.09, 2.83			6.1, 8.3
Met 6	7.97	4.70	2.19, 1.90	γ 2.51, γ′ 2.43		
Thr 7	8.05	4.43	4.63	γ(CH$_3$) 1.30	7.5	
Asp 8	8.66	4.45	2.92, 2.81			7.4, 7.5
Lys 9	8.42	3.95	1.84, 1.76	γ 1.54, γ′ 1.40, δ 1.67, ϵ 2.95, NH 7.52	4.0	8.6, 6.2
Glu 10	7.78	4.13	2.20	γ 2.55		
Cys 11	8.43	4.57	3.16			
Leu 12	8.03	3.98	1.76, 1.54	γ 1.66, δ 0.84, δ′ 0.81	4.0	9.6, 5.2
Tyr 13	7.61	4.22	3.03, 2.97	δ 6.79, ϵ 6.71	5.5	7.4, 9.3
Phe 14	8.52	4.28	3.22, 3.16	δ 7.45, ϵ 7.47, ζ 7.39		7.7, 9.0
Cys 15	8.46	4.75	3.17, 2.90		7.9	4.1, 10.3
His 16	7.88	4.62	3.36, 3.31	ϵ1 8.50, δ2 7.19	7.2	5.0, 8.8
Gln 17	8.06	4.30	2.07, 1.92	γ 2.25, NH 7.30, 6.74	7.4	5.0, 9.3
Asp 18	8.34	4.65	2.86, 2.70		7.5	6.0, 7.7
Val 19	7.84	4.03	1.85	γ 0.75, γ′ 0.61	8.1	
Ile 20	7.98	4.14	1.76	γ 1.38, γ′ 1.08, γ(CH$_3$) 0.81, δ 0.78	8.6	
Trp 21	8.00	4.65	3.33, 3.18	δ1 7.21, ϵ1 10.03, ϵ3 7.63, ζ2 7.43, ζ3 7.11, η2 7.18	7.7	5.3, 8.0

[a] Chemical shifts are reported in ppm, referenced to internal 3-trimethylsilylpropionic acid-d_4. [b] Coupling constants in Hz.

peptide was dissolved in water to give a solution of 37 μM at pH 6.6. Spectra were recorded in 0.1 cm pathlength cells at temperatures from 277 to 297 K at 4° intervals, on both the sample and on pure solvent, and the solvent blanks subsequently subtracted from the sample spectra. The temperature of the cell was controlled by a circulating water bath, and both the sample and the solvent blank were equilibrated for 10−15 min at each temperature prior to acquisition of the spectrum. Spectra were processed using the Jasco software in which a fast Fourier transform routine was employed to filter out low and high frequency noise. Results are expressed as mean residue ellipticities in units of deg cm^2 dmol^{-1}.

Sedimentation equilibrium experiments were performed on IRL 1620 using an XLA analytical ultracentifuge (Beckman Inst., Palo Alto, CA). A 3 mm column of the peptide solution from the NMR experiments was used in a 2.51 mm pathlength cell, with a home-made aluminium-filled epon centerpiece. The runs were performed at 60 000 rpm, at both 7 and 20 °C. The absorbance was recorded at 280 and 360 nm until the protein distribution in the cell was invariant over 3 h. The data were processed using the manufacturer's software, and the molecular weight was calculated assuming a partial specific volume of 0.73 mL g^{-1}.

RESULTS

SRTb. Sequence-specific assignments were made using the procedure developed by Wüthrich, as described previously (Mills et al., 1991). It has subsequently been found that SRTb aggregates at concentrations greater than 2.2 mM (Atkins et al., 1994), potentially causing ambiguities in the assignment of the NOE connectivities. Thus, the additional NMR experiments undertaken to refine the published structure for SRTb were acquired at a concentration of only 2.2 mM to eliminate the possibility of intermolecular NOEs. The chemical shifts are reported in Table 1, and a summary of the observed NOEs, and their distribution, is presented in Figure 1, panels A and B, respectively. Two hundred distance (87 intraresidue, 67 sequential, and 46 medium

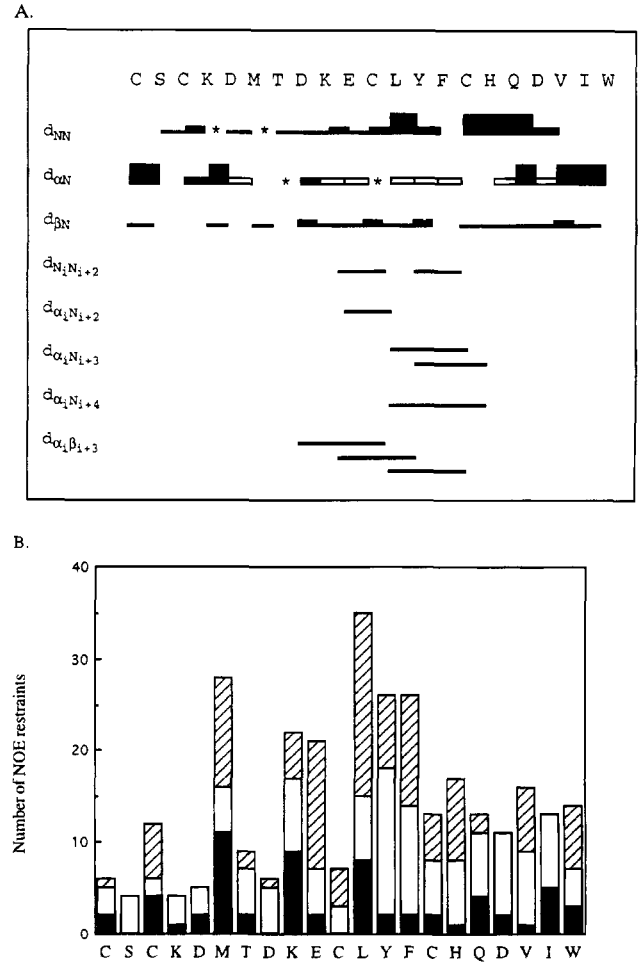

FIGURE 1: (A) Summary of NOEs observed for SRTb. The intensity of the NOE is depicted by the thickness of the line. An asterisk indicates that the NOE could not be unambiguously identified due to chemical shift overlap, and an open bar indicates that an NOE was observed but that the corresponding distance restraint did not constrain the geometry of the peptide and therefore was not used in the structure calculations. (B) Distribution of NOE restraints observed for SRTb. The solid bars correspond to the number of intraresidue NOEs, the open bars to sequential NOES, and the striped bars to medium- and long-range NOEs.

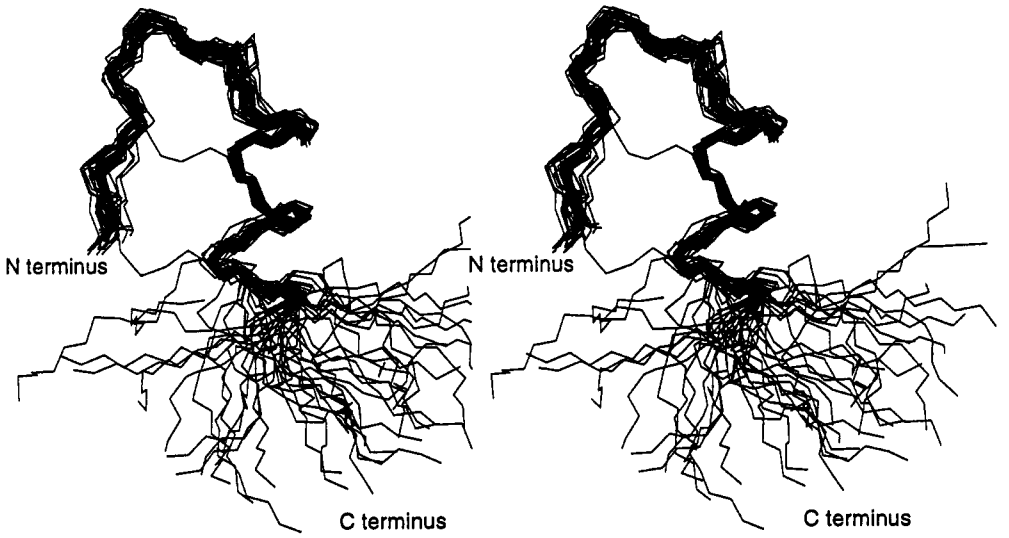

FIGURE 2: Stereo representation of the backbone conformations of 43 final structures of SRTb, overlaid over residues 1−3 and 8−16. The average RMSD for all structures over residues 1−16 was 0.78 Å for backbone atoms only and 1.39 Å for all heavy atoms.

range) and four torsion angle (Lys 9, Leu 12, and Ile 20 ϕ; Cys 1 χ_1) restraints were used to generate structures.

The efficiency of sampling of conformational space during structure generation was monitored using the angle order parameter, as defined by Hyberts et al. (1992), where complete sampling is indicated by a minimum in the order parameter. Well-defined angles are characterized by order parameters approaching 1.0, while for poorly defined angles the value approaches zero. It was found that after approximately 50 converged structures had been generated, the order parameters for the backbone torsion angles and the side chain χ_1 angles did not reduce significantly. Fifty initial structures were calculated, 43 of which were retained as acceptable structures using the criteria of no NOE violations greater than 0.4 Å, and no dihedral violations greater than 3°. In these final structures, the average energy due to NOE restraints violations was 6.5 ± 1.1 kcal mol^{-1}, and the average deviations from idealized covalent geometries were 0.0090 ± 0.0006 Å for bond length, 2.72 ± 0.05° for bond angle, and 0.19 ± 0.02° for the improper term.

The number of NOEs observed for each amino acid was uneven, with fewer NOEs detected for the terminal residues, suggesting that these residues are more mobile than the rest of the peptide. The orientation of the C-terminal residues with respect to the bicyclic structure appears unrestrained in the calculated conformations (Figure 2). This apparent structural heterogeneity can largely be attributed to two poorly defined angles in this region, Gln 17 ϕ and Asp 18 ψ, while the remaining angles are generally well-defined. Because of the additional restraints imposed by the disulfide bonds, the N-terminal residues appear to be structurally better defined than those of the C-terminus in Figure 2. The average RMSD, calculated for the superposition of the final 43 structures on an average structure over the defined region from residue 1 to 16, was 0.78 Å, SD 0.18 Å, for the backbone atoms only, and 1.39 Å, SD 0.22 Å, for all atoms.

The SRTb was found to adopt a well-defined helical conformation from residues 8 to 16, the average RMSD over just the helical residues for the 43 structures being only 0.40 Å, SD 0.16 Å, for the backbone heavy atoms. The ϕ and ψ angles for these residues were well-defined and lay close to the theoretical values for an α-helix. The amide proton resonances for Leu 12, Tyr 13, Phe 14, and Cys 15 were still observable after 1 h in D_2O at 303 K, consistent with the involvement of these residues in helix-stabilizing hydrogen bonds; however, hydrogen bond restraints were not used in the structure calculations because of the ambiguity of the hydrogen bond acceptors. Investigation of the hydrogen bond energy term, as given by X-PLOR, indicated that three of the expected bonds (Leu 12 NH−Asp 8 CO, Tyr 13 NH−Lys 9 CO, Cys 15 NH−Cys 11 CO) form with favorable energies in the calculated structures, but that the additional two expected hydrogen bonds were significantly less stable (Table 2). While the hydrogen bond parameters determined from structures calculated in the absence of solvent are necessarily approximate, the identified hydrogen bonds and their energies correlate well with the exchange data.

Table 2: Average Hydrogen Bond Energies in 43 SRTb Structures[a]

hydrogen bonds	number structures	energy (kcal/mol)
Cys11 HN−Thr7 CO	9	−2.92
Leu 12 NH−Asp 8 CO	43	−3.02
Tyr 13 NH−Lys 9 CO	42	−1.94
Phe 14 NH−Glu 10 CO	32	−0.65
Cys 15 NH−Cys 11 CO	41	−2.16
His 16 NH−Leu 12 CO	10	−0.59
Phe 14 NH−Cys 11 CO	22	−0.45
Gln 17 NH−Leu 12 CO	27	−1.49
Met 6 NH−Cys 3 CO	10	−0.53
Cys 11 NH−Thr 7 OG1	16	−0.83
Glu 10 NH−Thr 7 OG1	22	−1.69

[a] A hydrogen bond was identified when the energy, as measured in X-PLOR, was <−0.2 kcal/mol.

The SRTb sequence Thr^7-Glu^{10} agrees with the consensus sequence Thr/Ser-Xaa-Xaa-Glu proposed to function as an N-terminal helix stop signal, or Ncap (Harper *et al.*, 1993), where reciprocal hydrogen bonds form between the side chains and the backbone amide protons. The presence of Ncaps in peptides was confirmed by the identification of NOEs between the side chain protons of the glutamate and the amide of the Ncap (Zhou et al., 1994). We observed an NOE between the β protons of Glu 10 and the amide of Thr 7. An additional NOE was observed between the γ CH_3 of Thr 7 and the amide of Lys 9, which, from Zhou's proposed structure, may be close in a capping box. The proposed capping hydrogen bond between the amide of Glu 10 and the γ hydroxyl of Thr 7 (E10 NH−T7 OG1), was observed

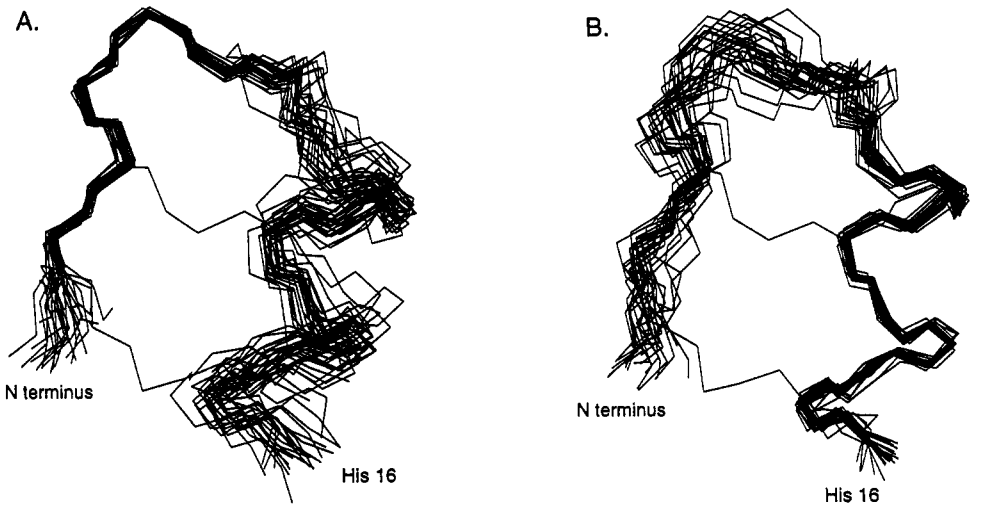

FIGURE 3: Superposition of 28 structures displaying a type $\beta_p\gamma$ turn; only residues 1−16 and the disulfide bonds of a single structure are displayed for clarity. (A) Structures superimposed over residues 2−6, average RMSD over the aligned residues 0.36 Å for backbone atoms, and 1.18 Å for all atoms. (B) Structures superimposed over the helical residues 8−16, average RMSD over aligned residues 0.38 Å for backbone atoms, and 1.16 Å for all atoms.

in 22 of the 43 calculated structures, with an average energy of −1.69 kcal mol^{-1}. The reciprocal hydrogen bond, between the carboxyl of Glu 10 and the amide of Thr 7 (E10 OE1/2−T7 NH), was observed in only eight structures. Harper et al. proposed that the characteristic geometry of the capping box was attributable to the nonhelical dihedral angles of the Ncap residue, which clustered around ϕ −94°, ψ +167° in Ncaps identified in structures in the Protein Data Bank. In 30% of the calculated SRTb structures identified as having the E10 HN−T7 OG1 hydrogen bond, the dihedral angles of Thr 7 were found to lie close to these values, and the α-helical hydrogen bond, C11 NH−T7 CO, formed with favorable energies (average energy −2.5 kcal mol^{-1}).

The angle order parameters indicate that the torsion angles Cys 3 ψ/Lys 4 ϕ, Thr 7 ψ/Asp 8 ϕ, and Gln 17 ϕ were poorly defined. A plot of the torsion angles Cys 3 ψ versus Lys 4 ϕ, however, clearly showed that the NOE restraints could be satisfied in two conformations, (+60°/−90°) and (−60°/+60°), and that these angles were in fact well-defined. In the case of Thr 7 ψ and Asp 8 ϕ, there was a dependence of Asp 8 ϕ on the preceding Thr 7 ψ; however, there were four broadly defined conformations (−140°/−120°, −60°/+180°, +30°/+60°, or +160°/−40°), providing this part of the sequence with a degree of variability. This variability is illustrated in Figure 3 which shows that the two segments Ser 2−Met 6 and Asp 8−His 16 are well-defined but are joined by a conformationally variable region. Gln 17 ϕ appears to adopt two preferred conformations (−135° or +60°) and is therefore an additional site of conformational variance. This variability is attributed to the lack of experimental restraints, and it is not known whether it reflects real conformational flexibility.

A turn was identified between residues Cys 3 and Met 6. In the majority of conformations (65%) the turn was a type II or $\beta_p\gamma$ turn as defined by Wilmot and Thornton (Wilmot et al., 1990) (Figure 3). The expected hydrogen bond associated with the turn was observed in 10 out of 28 structures and generally did not have favorable geometry, forming with an average energy of only −0.53 kcal mol^{-1}. In the remainding structures, a distorted $\alpha_L\gamma$ turn was observed. The distribution of the turn configurations reflects the variation in backbone torsion angles at Cys 3 ψ and Lys 4 ϕ, where +60°/−90° results in the formation of the $\beta_p\gamma$ turn.

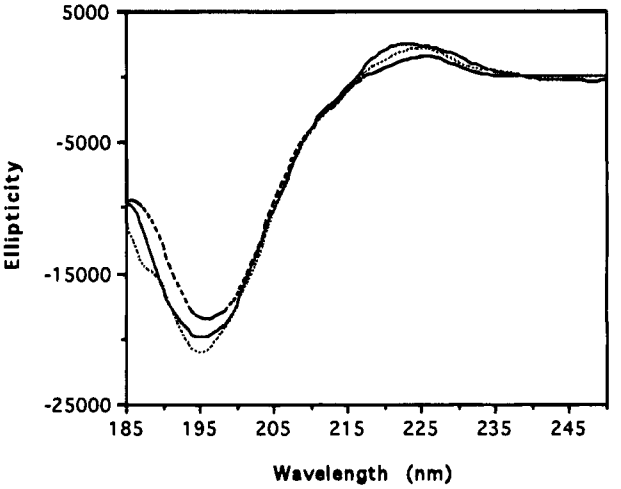

FIGURE 4: Circular dichroism spectra of IRL 1620, recorded at a peptide concentration of 37 μM in water at pH 6.6, in a 0.1 cm path length cell, averaged over five scans. The spectra recorded at 277 K (dark dashed line), 281 K (solid line), and 289 K (light dashed line) are shown. The spectrum at 285 K was almost identical to that recorded at 281 K and is not shown.

Analysis of the disulfide bond dihedral angles revealed that the 3 to 11 bridge showed a definite bias for left-handedness (91% of structures, average angle −87.0°, RMSD 15.5°). The 1 to 15 disulfide, however, showed little preference for the orientation of the bond (49% of structures left-handed, average angle −83.2°, RMSD 8.7°; 51% right-handed, average angle 81.8°, RMSD 7.7°). As mentioned earlier, the N-terminal residues have relatively few NOE restraints, which may be allowing sufficient flexibility in the calculated structures for the flipping of the 1 to 15 disulfide dihedral.

IRL 1620. The CD spectrum of IRL 1620 indicated that the structure was predominantly random coil. However, as the temperature was increased from 277 to 289 K, the absolute ellipticity at 195 nm increased, indicating an increase in coil content with temperature (Figure 4). As the temperature was further increased to 293 and 297 K, however, the absolute ellipticity at 195 nm decreased. Sedimentation equilibrium experiments showed that the peptide remained

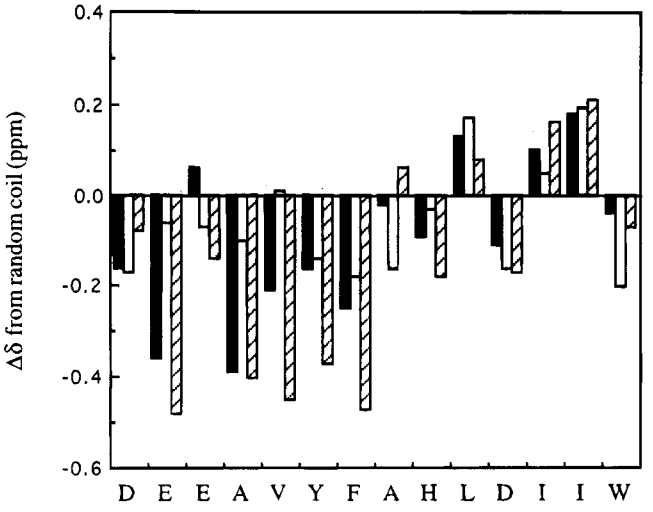

FIGURE 5: Differences in the chemical shift of the α protons of IRL 1620 (open bars), ET1 (striped bars) (Andersen et al., 1992a), and ET3 (solid bars) (Mills et al., 1992), from the values observed in random coil peptides.

monomeric up to concentrations that exceeded those used in the NMR experiments, thus eliminating aggregation as the origin of the changes in the CD spectrum. The observation of a temperature dependence of the CD spectrum implies that the conformation of the peptide at reduced temperatures is not completely random and that low populations of preferred conformers may exist in equilibrium with the unstructured peptide.

The conformations adopted by short peptides have been extensively studied, and criteria for identifying low populations of β turns via NMR have been developed (Dyson et al., 1991). Dyson proposed that several parameters be used in conjunction to predict the presence of turns, including reduced amide temperature coefficients, non-random-coil shifts for the α protons, reduced $^3J_{N\alpha}$ coupling constants, and the observation of specific NOEs. The NMR experiments on IRL 1620 were performed at reduced temperatures to increase the population of any structured conformers and to improve the NOE intensities.

The temperature coefficient for the amide proton may be correlated with the extent of protection from solvent exchange and has been shown to correlate with the predicted turn probability of individual amino acids (Dyson et al., 1988a). Reduced coefficients were measured for three residues in IRL 1620 (Glu 2 −5.7 ppb/°C, Glu 3 −5.5 ppb/°C, and Asp 11 −5.6 ppb/°C), but as these residues have the capacity to form intraresidue hydrogen bonds, these results must be interpreted with caution. The temperature coefficiences for the remaining residues were between −6.5 and −10.1 ppb/°C. It has been proposed for a rapidly interconverting mixture of conformers, where the conformational state can be modeled as a two-state equilibrium, that a linear correlation would exist between the amide temperature coefficient and the difference of the amide shift from random coil values (Andersen et al., 1992). No apparent correlation was detected for the IRL 1620 peptide, however.

The chemical shift of the α proton has been used as an indicator of secondary structure (Andersen et al., 1992b; Wishart et al., 1992), where three or four consecutive residues shifted by at least 0.1 ppm from the random coil values is indicative of a preferred conformation. The differences from random coil values (Wishart et al., 1992) of the IRL 1620 shifts are plotted in Figure 5 and are compared against the equivalent values for ET1 and ET3. Four residues in IRL 1620 from Ala 4 to Ala 8 were significantly shifted upfield, indicating a preference for the helical region of conformational space for these residues. Interestingly, the IRL 1620 shifts generally lie between those observed for the intact molecules and the random coil values.

In addition, the observation of three-bond coupling constants, $^3J_{NH\alpha}$, less than 5.5 Hz (Ala 4, Phe 7, and Ala 8) and greater than 8 Hz (Asp 11 and Ile 13) (Table 3) is not consistent with a rapidly interconverting conformation but indicates a preference for turns and extended structure, respectively.

Further evidence for the existence of low populations of structured conformers has been obtained from the observation of specific NOE interactions. The NOESY experiments at 280 and 284 K gave negative NOE peaks (summarized in Figure 6), which allowed sequence-specific assignments to be made (Table 3). Strong $\alpha_i N_{i+1}$ NOEs were observed, as expected for a largely extended structure; however, several NOEs were observed that were not consistent with a random structure and could not readily be rationalized as spin diffusion peaks. Where the shifts were sufficiently different, $N_i N_{i+1}$ peaks were observed, albeit weakly (Figure 7A). Close inspection of the spectra revealed the positive identification of four $\alpha_i N_{i+2}$ peaks, which have been found between the

Table 3. Chemical Shifts[a] and Coupling Constants[b] of IRL 1620 at 284 K and pH 6.6

	chemical shift				coupling constants	
residue	NH	αH	ββ′	others	$^3J_{N\alpha}$	$^3J_{\alpha\beta}$
Suc				2.55, 2.47		5.8, 8.3
Asp 1	8.33	4.59	2.71, 2.61		6.3	
Glu 2	8.59	4.23	2.07, 1.98	γ 2.30	6.0	
Glu 3	8.44	4.22	2.07, 1.98	γ 2.28	6.5	
Ala 4	8.23	4.25	1.37		5.2	
Val 5	8.01	3.96	1.96	δ 0.89, δ′ 0.77	7.3	
Tyr 6	8.14	4.46	2.90	δ 6.99, ε 6.77	6.3	
Phe 7	8.05	4.48	3.07, 2.91	δ 7.22, ε 7.34, ζ 7.22	5.3	5.6, 8.6
Ala 8	8.13	4.19	1.33		4.6	
His 9	8.29	4.60	3.20, 3.15	δ2 7.18, ε1 8.35	7.2	5.3, 9.0
Leu 10	8.17	4.34	1.59, 1.54	γ 1.53, δ 0.89, δ′ 0.84	7.3	9.3, 5.0
Asp 11	8.42	4.60	2.68, 2.56		8.1	5.9, 8.3
Ile 12	7.96	4.00	1.67	γ 1.36, γ′ 1.04, γ(CH_3) 0.49, δ 0.77	7.9	
Ile 13	8.06	4.14	1.78	γ 1.36, γ′ 1.10, γ(CH_3) 0.83, δ 0.81	8.5	
Trp 14	7.80	4.50	3.32, 3.12	δ1 7.22, ε1 10.07, ε3 7.70, ζ2 7.47, ζ3 7.15, η2 7.23	7.9	4.6, 8.3

[a] Chemical shifts are reported in ppm, referenced to internal 3-trimethylsilylpropionic acid-d_4. [b] Coupling constants are reported in Hz.

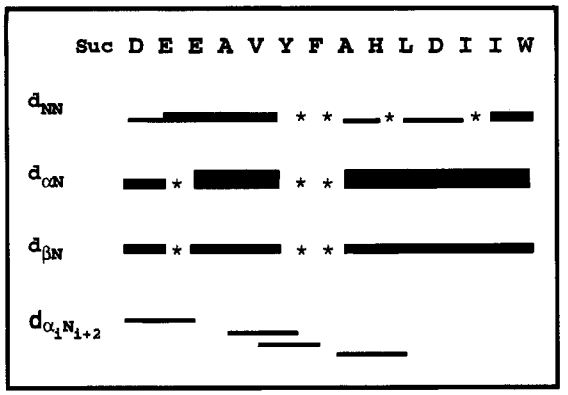

FIGURE 6: Summary of NOEs observed for IRL 1620. The intensity of the NOE is depicted by the thickness of the line. An asterisk indicates that the NOE could not be unambiguously identified due to chemical shift overlap.

second and fourth residues across β turns (Dyson et al., 1988a). The existence or otherwise of additional $\alpha_i N_{i+2}$ peaks could not be established because of spectral overlap. In addition, side chain to backbone NOEs were observed (Figure 7B) and are listed in Table 4.

The combined evidence of nonrandom α proton chemical shifts and coupling constants, and the observation of medium-range NOEs, point to the existence of a series of overlapping turn-like structures between residues Glu 3 and His 9, in equilibrium with extended or random coil structures.

DISCUSSION

The helix characterized in SRTb, and previously in the endothelin peptides, is well-defined, if irregular. The specific topology of the disulfide bridges of these peptides is known to stabilize helical conformations (Pease et al., 1990), and the presence of an Ncap in the SRTb sequence has also been predicted to increase the helical content. Removal of the disulfides, and the consequent destabilization of the helix, reduced the binding of the intact peptides to the selective ET_A receptors (Saeki et al., 1991), thereby implicating the helical conformation in this specific receptor interaction. The high sequence homology from residues 8 to 21, and the presence of the helix in most calculated ET and SRT structures, suggests that the specificity of interaction of ligands with this receptor is determined partly by the variable region between residues 4 and 7. We have located the turn in the SRTb peptide to residues Cys 3−Met 6, as suggested by Aumelas et al. (1991), rather than residues 5−8 as seen in ET1. This provides evidence for a conformational difference in this region of the peptide which may be partly responsible for the lower binding affinity to the ET_A receptor of SRTb compared to ET1. Andersen et al. (1992a) identified sites of conformational variance in the ET1 structure at residues 3/4 and 8/9. In SRTb, the 3/4 peptide bond displayed a similar conformational variability; however, the 7/8 bond, rather than the 8/9 bond, was found to be the second variable region, resulting in further differences between the endothelin and sarafotoxin structures in the variable loop region.

The recently published crystal structure of ET1 (Janes et al., 1994) described the conformation of the variable loop region as a bulged out face of an extended sheet. These findings are not consistent with ours, or those of others. However, Janes et al. described intermolecular contacts between the N terminus of one molecule and residues 5−8 of another, as well as distortions of the ϕ and ψ angles in residue 8. It is possible that the observed differences between the structures can be attributed to these intermolecular interactions in the crystal.

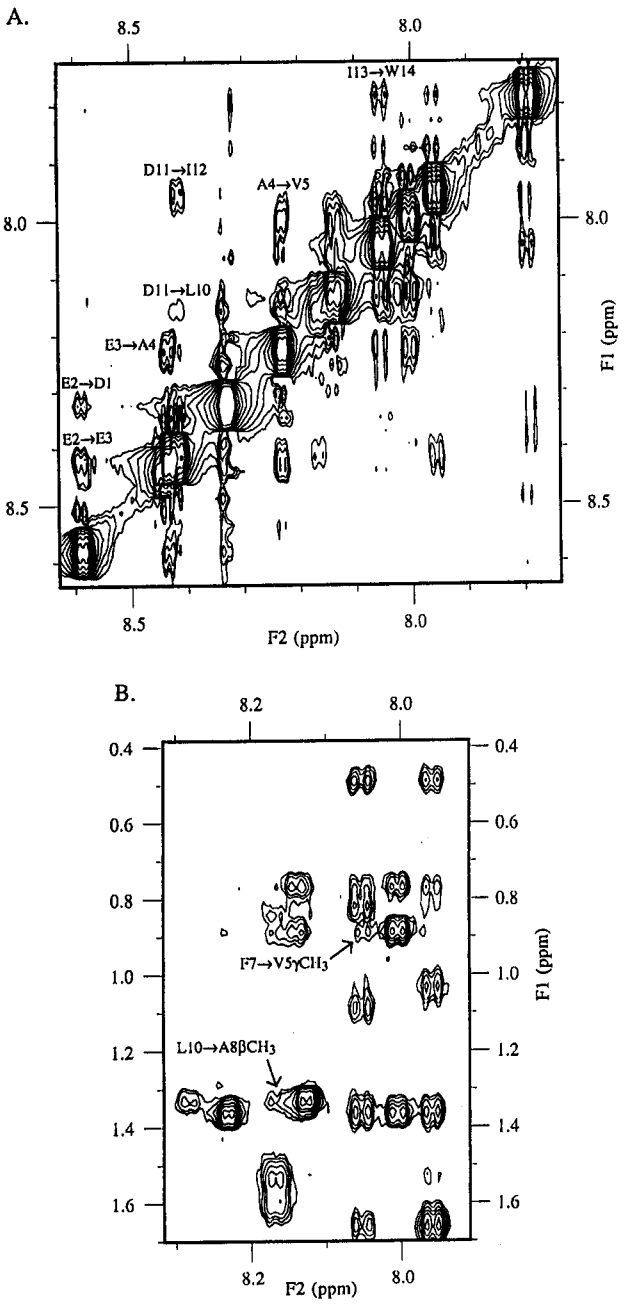

FIGURE 7: NOESY spectrum of a 2.4 mM solution of IRL 1620, recorded at pH 6.6, 284 K on a Bruker AMX500 spectrometer using a 350 ms mixing time. The F_2 dimension was plotted as the horizontal axis, F_1 as the vertical axis. (A) Region containing the NN cross peaks. (B) Region containing the amide to side chain NOEs with the nonsequential peaks labeled.

Table 4: Nonsequential NOEs Observed for IRL 1620 at 280 and 284 K

$\alpha_i N_{i+2}$	medium-range NOEs
D1αE3HN	V5α A8HN
A4αY6HN	V5α A8Qβ
V5αF7HN	V5Qγ1 F7HN
A8αL10HN	A8Qβ L10HN
	I12Qγ2 W14HN
	I12Qγ2 W14α
	I12Qγ2 W14Hε3

The conformation of the C-terminal residues in SRTb could not be determined due to the lack of medium- or long-range interactions, as has been found in most previous studies of the ET/SRT molecules. In contrast, an irregular helix was identified between residues 12 and 21 in the crystal structure (Janes et al., 1994).

The truncated analogue, IRL 1620, lacks the helix-stabilizing disulfide bonds [to some extent counteracted by the substitution of the cysteines by the helix-favoring alanine (Marqusee et al., 1989)] and the correct geometry for the formation of the Ncap, binds weakly to the selective ET_A receptor, but binds with high affinity to the nonselective ET_B receptor. Our studies have shown that although the peptide conformation is predominantly random coil, there is evidence that preferred conformations exist at reduced temperatures. The evidence is consistent with the N-terminal residues adopting a series of overlapping turn conformations, or a nascent helix (Dyson et al., 1988b), in the part of the sequence corresponding to the helical region of the intact peptides. The high association constant for IRL1620 (Takai et al., 1992) implies that there are very specific and strong interactions with the ET_B receptor despite the fact that it is largely unstructured when free in solution: this implies either that the receptor recognises the small proportion of agonist molecules that possess all or part of the helical segment or that a more ordered conformation is induced on binding. In the former case, IRL 1620 would bind to the ET_B receptor in a similar fashion to the intact molecules with its N-terminal residues, which are necessary for high affinity binding (Takai et al., 1992), adopting a favorable disposition for recognition by the receptor.

ACKNOWLEDGMENTS

We are grateful to Dr. G. F. King, the University of Sydney, for discussions, to Dr. I. D. Campbell for his assistance during A.R.A.'s tenure of a British Council Bursary at the Biochemistry Department, the University of Oxford, Dr. D. Doak, Biochemistry Department, University of Oxford, for sharing his X-PLOR script for determining the angle order parameters, and Mr. M. Jacobsen, the University of Queensland, for running the sedimentation experiments.

REFERENCES

Andersen, N. H., Chen, C., Marschner, T. M., Krystek, S. R., & Bassolino, D. A. (1992a) *Biochemistry 31*, 1280−1295.
Andersen, N. H., Cao, B., & Chen, C. (1992b) *Biochem. Biophys. Res. Commun. 184*, 1008−1014.
Atkins, A. R., Ralston, G. B., & Smith, R. (1994) *Int. J. Pept. Protein Res. 44*, 372−377.
Aumelas, A., Chiche, L., Mahe, E., & Le-Nguyen, D. (1991) *Neurochem. Int. 18*, 471−475.
Bennes, R., Calas, B., Chabrier, P., Demaille, J., & Heitz, F. (1990) *FEBS Lett. 276*, 21−24.
Bortmann, P., Hoflack, J., Pelton, J. T., & Saudek, V. (1991) *Neurochem. Int. 18*, 491−496.
Braunschweiler, L., & Ernst, R. R. (1983) *J. Magn. Reson. 53*, 521−528.
Brunger, A. T. (1992) X-PLOR Version 3.1, Yale University, New Haven, CT.
Dyson, H. J., & Wright, P. E. (1991) *Annu. Rev. Biophys. Biophys. Chem. 20*, 519−538.
Dyson, H. J., Rance, M., Houghten, R., Lerner, R. A., & Wright, P. E. (1988a) *J. Mol. Biol. 201*, 161−200.
Dyson, H. J., Rance, M., Houghten, R., Wright, P. E., & Lerner, R. A. (1988b) *J. Mol. Biol. 201*, 201−217.
Eccles, C., Güntert, P., Billeter, M., & Wüthrich, K. (1991) *J. Biomol. NMR 1*, 111−130.
Gill, S. C., & von Hippel, P. H. (1989) *Anal. Biochem. 182*, 319−326.
Harper, E. T., & Rose, G. D. (1993) *Biochemistry 32*, 7605−7609.
Hyberts, S. G., Goldberg, M. S., Havel, T. F., & Wagner, G. (1992) *Protein Sci. 1*, 736−751.
Janes, R. W., Peapus, D. H., & Wallace, B. A. (1994) *Nature, Struct. Biol. 1*, 311−319.
Jeener, J., Meier, B. H., Bachmann, P., & Ernst, R. R. (1979) *J. Chem. Phys. 71*, 4546−4553.
Karne, S., Jayawickreme, C. K., & Lerner, M. R. (1993) *J. Biol. Chem. 268*, 19126−19133
Kloog, Y., Ambar, I., Sokolovsky, M., Kochva. E., Wollberg, Z., & Bdolah, A. (1988) *Science. 242*, 268−270.
Marion, D., & Wüthrich. K. (1983) *Biochem. Biophys. Res. Commun. 113*, 967−974.
Marqusee, S., Robbins, V. H., & Baldwin, R. L.(1989) *Proc. Natl. Acad. Sci. U.S.A. 86*, 5286−5290.
Mills, R. G., Atkins, A. R., Harvey, T., Junius, F. K., Smith, R., & King. G. F. (1991) *FEBS Lett. 282*, 247−252.
Mills, R. G., O'Donoghue, S. I., Smith, R., & King, G. F. (1992) *Biochemistry 31*, 5640−5645.
Mills, R. G., Ralston, G. B., & King, G. F. (1994) *J. Biol. Chem.* (in press).
O'Donnell, S. R., Kay, C. S., Atkins, A. R., & Smith, R. (1993) *Pharmacol. Commun. 4*, 1−10.
Pease, J. H. B., Storrs, R. W., & Wemmer, D. E. (1990) *Proc. Natl. Acad. Sci. U.S.A. 87*, 5643−5647.
Pelton, J. T. (1991) *Neurochem. Int. 18*, 485−489.
Pelton, J. T., & Miller, R. C (1991) *J. Pharm. Pharmacol. 43*, 43−45.
Rance, M., Sørensen, O. W., Bodenhausen, G., Wagner, G., Ernst, R. R., & Wüthrich, K. (1983) *Biochem. Biophys. Res. Commun. 117*, 479−483.
Reily, M. D., & Dunbar, J. B. (1991) *Biochem. Biophys. Res. Commun. 178*, 570−577.
Saeki, T., Ihara, M., Fukuroda, T., Yamagiwa, M., & Yano. M. (1991) *Biochem. Biophys. Res. Commun. 179*, 286−292.
Sarin, V. K., Kent, S. B. H., Tam, J. P., & Merrifield, R. B. (1981) *Anal. Biochem. 117*, 147−157.
Saudek,V., Hoflack, J., & Pelton. J. T. (1989) *FEBS Lett. 257*, 145−148.
Saudek, V., Hoflack, J., & Pelton, J. T. (1990) *Int. J. Pept. Protein Res. 37*, 174−179.
Schnölzer, M., Alewood, P., Jones, A., Alewood, D., & Kent, S. B. H. (1992) *Int. J. Pept. Protein Res. 40*, 180−193.
Sokolovsky, M. (1992) *J. Neurochem. 59*, 809−821.
Takai, M., Umemura, I., Yamasaki, K., Watakabe, T., Fujitani, Y., Oda, K., Urade, Y., Inui, T., Yamamura, T., & Okada, T. (1992) *Biochem. Biophys. Res. Commun. 184*, 953−959.
Tamaoki, H., Kobayashi, Y., Nishimura, S., Ohkubo, T., Kyogoku, Y., Nakajima, K., Kumagaye, S., Kimura, T., & Sakakibara, S. (1991) *Protein Eng. 4*, 509−518.
Tamaoki, H., Kyogoku, Y., Nakajima, K., Sakakibara, S., Hayashi, M., & Kobayashi, Y. (1992) *Biopolymers 32*, 353−356.
Wilmot, C. M., & Thornton, J. M. (1990) *Protein Eng. 3*, 479−493.
Wishart, D. S., Sykes, B. D., & Richards, F. M. (1992) *Biochemistry 31*, 1647−1651.
Wüthrich, K., Billeter, M., & Braun, W. (1983) *J. Mol. Biol. 169*, 949−961.
Yanagisawa, M. Kurihara, H., Kimura, S., Tomobe, Y., Kobayashi, M., Mitsui, Y., Yazaki, Y., Goto, K., & Masaki, T. (1988) *Nature 332*, 411−415.
Zhou, H. X., Lyu, P., Wemmer, D. E., & Kallenbach, N. R. (1994) *Proteins: Struct., Funct., Genet. 18*, 1−7.

BI942154V